Motion is Inevitable: The Impact of Motion Correction Schemes on HARDI Reconstructions

Shireen Elhabian, Yaniv Gur, Clement Vachet, Joseph Piven for IBIS*, Martin Styner, Ilana Leppert, G. Bruce Pike and Guido Gerig

Abstract Diffusion weighted imaging (DWI) is known to be prone to artifacts related to motion originating from subject movement, cardiac pulsation and breathing, but also to mechanical issues such as table vibrations. Given the necessity for rigorous quality control and motion correction, users are often left to use simple heuristics to select correction schemes, but do not fully understand the consequences of such choices on the final analysis, moreover being at risk to introduce confounding factors in population studies. This paper reports work in progress towards a com-

Shireen Elhabian, Yaniv Gur, Clement Vachet and Guido Gerig
Scientific Computing and Imaging Institute, Salt Lake City, UT, USA, e-mail: {shireen, yanivg, cvachet, gerig}@sci.utah.edu

Joseph Piven
Dept. of Psychiatry, University of North Carolina, NC, USA, e-mail: jpiven@med.unc.edu

Martin Styner
Dept. of Psychiatry and Dept. of Computer Science, University of North Carolina, NC, USA, e-mail: styner@unc.edu

Ilana Leppert
Dept. of Neurology and Neurosurgery, Montral Neurological Institute, Montral, Quebec, Canada, e-mail: ilana@bic.mni.mcgill.ca

G. Bruce Pike
Dept. of Neurology and Neurosurgery, Montral Neurological Institute, Montral, Quebec, Canada, Dept. of Radiology, University of Calgary, Calgary, Canada, e-mail: bruce.pike@mcgill.ca

* This work is supported by NIH grants ACE RO1 HD 055741 and NA-MIC Roadmap U54 EB005149 and the cocaine infant project (CAMID NIDA DA022446-01). *The NIH funded Autism Centers of Excellence Infant Brain Imaging Study (ACE-IBIS) Network: Clinical Sites: University of North Carolina: J. Piven (IBIS Network PI), H.C. Hazlett, C. Chappell; University of Washington: S. Dager, A. Estes, D. Shaw; Washington University: K. Botteron, R. McKinstry, J. Constantino, J. Pruett; Children's Hospital of Philadelphia: R. Schultz, S. Paterson; University of Alberta: L. Zwaigenbaum; Data Coordinating Center: Montreal Neurological Institute: A.C. Evans, D.L. Collins, G.B. Pike, V. Fonov, P. Kostopoulos; Samir Das; Image Processing Core: University of Utah: G. Gerig; University of North Carolina: M. Styner; Statistical Analysis Core: University of North Carolina: H. Gu.

prehensive evaluation framework of HARDI motion correction to support selection of optimal methods to correct for even subtle motion. We make use of human brain HARDI data from a well controlled motion experiment to simulate various degrees of motion corruption. Choices for correction include exclusion or registration of motion corrupted directions, with different choices of interpolation. The comparative evaluation is based on studying effects of motion correction on three different metrics commonly used when using DWI data, including similarity of fiber orientation distribution functions (fODFs), global brain connectivity via Graph Diffusion Distance (GDD), and reproducibility of prominent and anatomically defined fiber tracts. Effects of various settings are systematically explored and illustrated, leading to the somewhat surprising conclusion that a best choice is the alignment and interpolation of all DWI directions, not only directions considered as corrupted.

Key words: Diffusion MRI, HARDI, subject motion, motion correction, fiber orientations, orientation distribution functions, tractography comparison, impact quantification

1 Introduction

In today's clinical diffusion-weighted (DW)-MRI acquisitions, subject motion is considered one of the most relevant sources of noise artifacts [1], ranging from physiological motion such as cardiac pulsation, to physical (voluntary or involuntary) movement by the patient. While physiological motion can be controlled by gating or in the sequence design, the physical patient movement during the diffusion-encoding gradient pulses leads to severe signal perturbation which results in a significant signal phase shift, or signal loss [2].

During a scanning session, the degree of patient's cooperation may vary. For example, elderly people who may become uncomfortable during large scanning sessions, patients in pain who become restless and agitated during a scan and unsedated pediatric subjects who will not cooperate long enough to be imaged without motion artifacts, to name a few. As such, it is safe to assume that there are always motion artifacts in any given DW-MRI acquisition, a proof-of-concept of this hypothesis being presented in 2.1.1.

Motion effects can be reduced by real-time motion detection [3, 4], where the acquisition and the source of motion are synchronized so that the data is never corrupted. However, this prospective approach for motion correction might affect the acquisition time. Further there is no guarantee that the head will ever move back to the original position. Alternatively, the exclusion of one or more gradients bearing strong motion artifacts can be exercised [5], a.k.a motion scrubbing in functional MRI, however, this limits the ability to reconstruct crossing fibers especially at small separation angles. As such, post-acquisition motion correction is imperative to guarantee voxel-wise correspondence between different DWIs referring to the same anatomical structure. A common practice is to heuristically select trans-

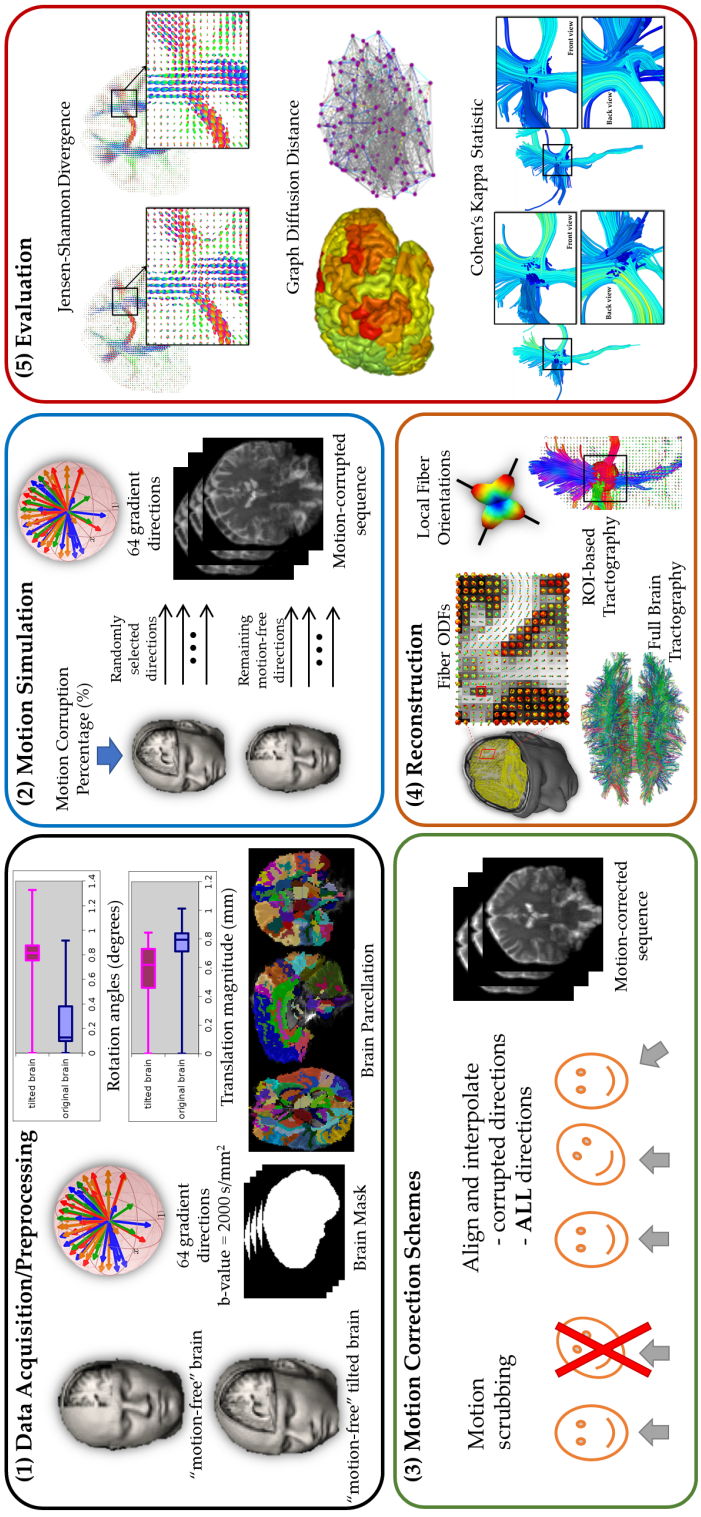

Fig. 1 Experimental framework for subject motion simulation and HARDI-based reconstructions evaluation

formation parameter thresholds for detection of motion outliers, where registration and interpolation is applied to gradient directions that are claimed to be corrupted.

To mitigate motion artifacts, raw DWIs are usually co-registered to the least diffusion-weighted images using rigid transformation. Software packages for image-based registration of DWIs are becoming readily available, e.g. FSL-MCFLIRT [6], the Advanced Normalization Tools (ANTS) [7], TORTOISE [8] and DTIPrep [9]. Nonetheless, the interpolation step of a typical registration approach has been shown to significantly change the noise properties of DWIs [10].

The optimal pre-processing pipeline for HARDI sequences remains an open question and a challenge on real data. For example, is there a threshold that would identify a motion-corrupted volume? How sensitive are HARDI reconstructions to such a pre-defined threshold? What is the impact of various motion-correction schemes on subsequent HARDI-based reconstructions and tractography? So far, these issues have received, surprisingly, little attention in various DW-MRI studies of clinical populations.

This study does not focus on the closeness of HARDI-based reconstructions to an existing truth, but on the effect of pre-processing schemes, in particular motion correction, commonly deployed as a post-acquisition step, on succeeding steps. In this paper, we propose a comprehensive experimental framework (see Figure 1) that enables making use of human brain HARDI data from a well controlled motion experiment to simulate various degrees of motion corruption. Choices for correction include scrubbing or registration of motion corrupted directions, with different choices of interpolation, and also the option of registration/interpolation of all directions. The comparative evaluation covers three different metrics, including similarity of fiber orientation distribution functions (fODFs) via Jensen-Shannon divergence (JSD), global brain connectivity via Graph Diffusion Distance (GDD), and reproducibility of four anatomically-defined fiber pathways via Cohen's Kappa statistics.

On the basis of our findings, we recommend assuming there is always motion, even subtle, in the acquired scans. As such, motion correction needs to be applied to all gradient directions without relying heuristically on a threshold which determines a gradient direction to be claimed as motion corrupted.

2 Materials and Methods

2.1 Phantom Acquisition

2.1.1 Proof-of-Concept:

To backup our assumption that motion is omnipresent, we analyze data from three healthy human volunteers (males 30-40 years-old) visiting four clinical sites where they signed a generic consent form at each site agreeing to be scanned for research purposes. Each subject was scanned twice on a 3T Siemens Tim Trio scanner with a strict calibration of image acquisition parameters. The scanning environment was well controlled, a comfortable padding was used to minimize head motion while

urging participants to remain without movement. Eddy current was compensated by using a Twice-refocused Spine Echo (TRSE) protocol, with FoV = 209mm, 76 transversal slices, thickness = 2mm, $(2mm)^3$ voxel resolution, matrix size = 106^2, TR = 11100ms, TE = 103ms, one baseline image with zero b-value and 64 DWI with b-value at 2000 s/mm^2, with total scan time of 12.5 minutes.

FSL-MCFLIRT [6] was then used to provide the rigid transformation matrix (6 DOF) for each image volume having the baseline image as the reference for motion correction and normalized mutual information as the cost function. To quantify motion, we used the magnitude of the translation vector (in mm) as well as the axis-angle rotation representation (in degrees). The boxplots in Fig. 2 show the rotational and translational components of the motion being detected from a total of 24 DWI datasets. This shows an experimental proof of the existence of quantifiable motion (on average 0.39^o rotation and 0.61mm translation), even subtle, in the acquired HARDI data. The graphs in Fig. 2 illustrate the arbitrariness of common calculation of percentage of motion corruption, here shown as a function of thresholding on the estimated motion parameters.

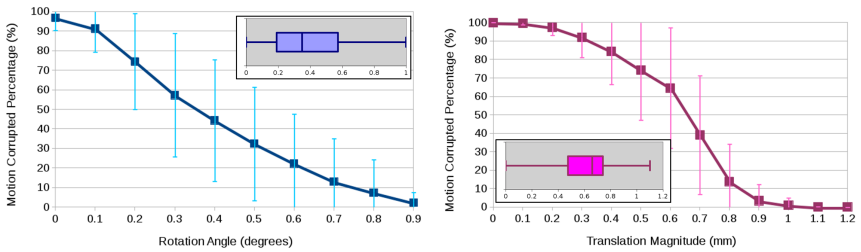

Fig. 2 Average and standard deviation of the percentage of motion-corrupted gradient directions as a function of thresholding on the estimated rotation angle in degrees (left) and the estimated translation magnitude in mm (right) for three human phantoms scanned twice at four clinical sites. The boxplots show the overall statistics of estimated motion parameters.

2.1.2 Atlas-Guided White Matter Parcellation:

For automated placement of 3D region-of-interests (ROIs) defining seeds for tractography and connectivity, we used the publicly available JHU-DTI-SS (a.k.a. "Eve") atlas described in [11], which includes 176 core and peripheral ROIs. To reduce variability introduced by individual parcellation in subject space, we defined a common reference for our population (multiple acquisitions of the same phantom). This is achieved by generating an unbiased average and diffeomorphic deformations from the sets of images (using tensor maps extracted from HARDI). The "Eve" Fractional Anisotropy (FA) atlas was registered to FA images of the phantom-specific atlases using the ANTS [7] tool, along with mapping of the "Eve" white matter labels. Finally, "Eve" labels were mapped back to coordinates of original HARDI data by inverse diffeomorphic transforms.

2.1.3 Human Motion Simulation:

As a pilot, one human phantom was asked to be re-scanned while having the head tilted to simulate noticeable motion. The two datasets were then used to construct motion-corrupted sequences. Based on alignment of the baseline images of the two scans (original and tilted) using FSL-MCLFIRT, 12^o rotation and 7 *mm* translation were detected, while less than 1^o of rotation and 0.8*mm* of translation were found when aligning individual DWIs to their corresponding baseline image. We arbitrarily considered the first out of the two scans as the "motion-free" sequence and used it as a reference for performance evaluation of different motion correction schemes. A random percentage of DW images (10, 30, 50, 70 and 90%, each with 10 different random sets of gradient directions) drawn from the second scan (tilted brain) were mixed with the first scan to construct 50 motion-corrupted datasets (10 experiments times 5 corruption percentages).

2.1.4 Motion Correction Schemes:

We explored three motion correction schemes. In the first approach, we follow the motion scrubbing approach, usually deployed in functional MRI, where we exclude the affected gradient directions from subsequent computations (i.e., diffusion profile reconstruction and tractography). In the second approach, we only align and interpolate the corrupted gradient directions. This mimics the situation where a pre-defined motion parameter threshold is used to claim whether a DWI volume is motion-corrupted. Note that the diffusion gradient vectors corresponding to the corrupted volumes are re-oriented to incorporate the rotational component of subject motion. In the third approach, assuming there is always motion, we force the alignment and interpolation of all DWI volumes while the respective gradient vectors are re-oriented accordingly. The interpolation step in the second and third approaches was performed using FSL-MCFLIRT [6] with nearest neighbor, trilinear, sinc and spline interpolants.

2.2 Reconstruction and Tractography

We employed the constrained spherical deconvolution (CSD) technique [12] to reconstruct fODFs using the DiPy library [13]. We used spherical harmonics representation of order 8 which was kept constant for all our experiments. Full brain tractography was performed using the EuDX deterministic tracking technique [14] (implemented in the DiPy library), using random seeding inside the brain region and a turning-angle threshold of 30^o between two connected voxels. The fODFs and tractography were computed for the 450 motion corrected sequences (50 datasets times 9 correction schemes), as well as the motion-free sequence.

Further, a multi-ROI approach was used to reconstruct four prominent and previously well-described fiber pathways using the Template ROI set (TRS) defined

in [15] which exploits the existing anatomical knowledge of tract trajectories. The TRS (pass through and not-pass through) of four fundamental fiber bundles (left and right hemispheres) were defined based on "Eve" atlas-based parcellation of the original DWI images. We report the matching results from the four bundles as defined in [15]: the cortical spinal tract (CST), the inferior fronto-occipital tract (IFO), the inferior longitudinal fasciculus (ILF), and the uncinate fasciculus (UNC).

2.3 Evaluation Metrics

2.3.1 Voxel-based Metric:

Similarities between the original motion-free fODFs and the fODFs corresponding to the motion corrected images were measured using the Jensen-Shannon divergence (JSD), which has been used to quantify differences between ODFs in various studies [16].

2.3.2 Global Connectivity-based Metric:

We used the 176 core and peripheral ROIs defined in the white matter parcellation (see 2.1.2) to compute weighted connectivity graphs from the full brain tractography result. The edge weights were inversely proportional to the tracts lengths giving a higher connection strength to short tracts to compensate for signal attenuation. The brain connectivity graphs were then compared by means of the recently proposed graph diffusion distance (GDD) metric [17], which takes into account the graph structure in addition to the edge weights.

2.3.3 Tract-based Metric:

The spatial matching between motion-free and motion-corrected tracts was examined using Cohen's Kappa statistic [18]. The Kappa statistic measures the level of agreement of the tracking results (determined by cross-tabulating tract detection for two given tracking results) and corrects for agreement that would be expected by chance (determined by the marginal frequencies of each tracking result).

3 Results and Discussion

The average JSD metric was computed using the fODF reconstruction from the raw dataset not corrupted by mixing DWI directions from the tilted-brain scan as a reference (i.e. only presenting subtle motion inherent to a scan). We differentiated between regions where multiple fibers were detected versus single fiber regions. Fig-

ure 3 shows the average JSD values for single and multiple fiber regions as a function of motion corrupted percentage. As anticipated, heterogeneous regions are more affected (showing larger average JSD) by the interpolation step of motion correction in general when compared to that of single fiber regions, regardless of the interpolation scheme employed. It can be observed that the impact of motion scrubbing (removing gradient directions) becomes more pronounced when compared to interpolation. The JSD values indicate minimal deformations in fODFs reconstructed after forcing the alignment and interpolation of all gradient directions.

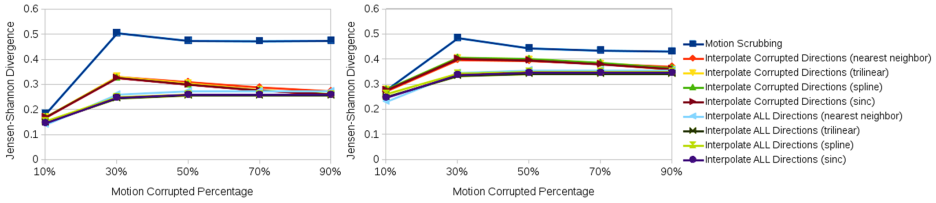

Fig. 3 The average Jensen-Shannon divergence (JSD) values for single fiber regions (left) and for multiple fiber regions (right)

Figure 4(left) shows the average GDD metric computed based on the weighted connectivity graphs from tractography result based on raw scan reconstructions versus that of motion-corrected ones. One may observe consistent findings when compared to the JSD metric; the global brain connectivity is least affected by the motion correction step when forcing the alignment and interpolation of all gradient directions without setting a pre-defined threshold to claim corrupted volumes. Although excluding corrupted gradients might seem an alternative choice for motion correction, the connectivity graphs show high deviations (larger GDD) especially when the percentage of directions being corrupted is increased.

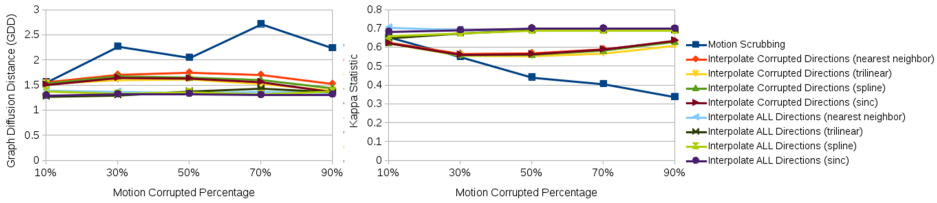

Fig. 4 Left: Average Graph Diffusion Distance (GDD). Right: Average Cohen's Kappa statistic for the cortical spinal tract (CST) for the left hemisphere.

Figure 4(right) shows the average Kappa statistic computed from the CST tract in the left hemisphere (other fiber tracts showed similar trends, yet their graphs were omitted due to space limitation). Being consistent with the results from JSD and GDD metrics, motion scrubbing shows a significant decrease in the degree of

tract agreement when increasing percentage of motion corruption which in turn yields discarding more gradient directions. Nonetheless, the maximal agreement is achieved when aligning and interpolating all gradient directions to correct for motion, even if considered subtle, see Figure 5 for a sample tractography result. One can observe that the detected tracts when corrupted gradients are excluded deviate from being anatomically realistic. This is due to insufficient number of gradients and unbalanced sampling of the q-space.

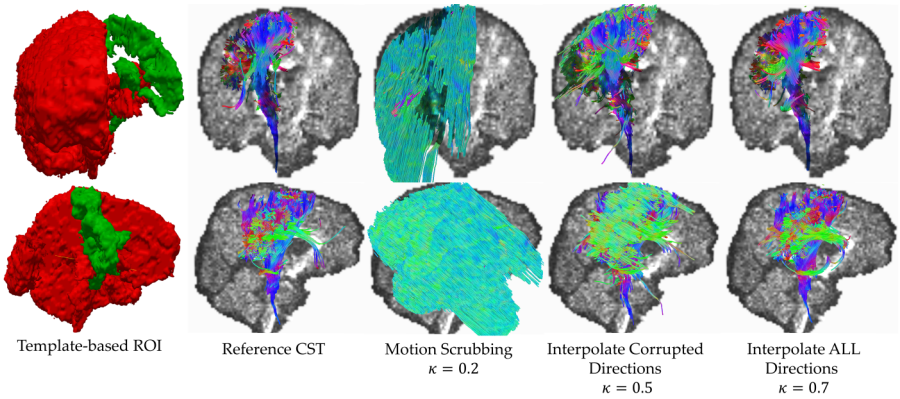

Fig. 5 Sample tractography result for the cortical spinal tract (CST) (left hemisphere) with 50% motion corruption.

4 Conclusion

Although there is excellent theoretical work on DWI acquisition parameters and ODF reconstruction schemes, as well as its effects on the quality and crossing fiber resolution, standard users lack clear guidelines and recommendations on the best ways to approach and correct for motion in practical settings. This work investigates motion correction using transformation and interpolation of affected DWI directions versus the exclusion of subsets of DWIs, and its impact on the reconstructed fODFs, on brain connectivity and on the detection of fiber tracts. The various effects are systematically explored and illustrated via living phantom data, leading to the conclusion that motion, even subtle, exists in every acquired DW scan while subsequent reconstructions are least affected by the motion correction step when forcing the alignment and interpolation of all gradient directions without setting pre-defined thresholds to claim corrupted volumes.

References

1. Pierpaoli, C.: Artifacts in diffusion MRI. Diffusion MRI: Theory, Methods and Applications, Oxford University Press, New York (2010) 303–318
2. Tournier, J.D., Mori, S., Leemans, A.: Diffusion tensor imaging and beyond. Magnetic Resonance in Medicine **65**(6) (2011) 1532–1556
3. Caruyer, E., Aganj, I., Lenglet, C., Sapiro, G., Deriche, R.: Motion detection in diffusion MRI via online odf estimation. International journal of biomedical imaging **2013** (2013)
4. Kober, T., Gruetter, R., Krueger, G.: Prospective and retrospective motion correction in diffusion magnetic resonance imaging of the human brain. Neuroimage **59**(1) (2012) 389–398
5. Liu, Z., Wang, Y., Gerig, G., Gouttard, S., Tao, R., Fletcher, T., Styner, M.: Quality control of diffusion weighted images. In: SPIE Medical Imaging, International Society for Optics and Photonics (2010) 76280J–76280J
6. Jenkinson, M., Bannister, P., Brady, M., Smith, S.: Improved optimization for the robust and accurate linear registration and motion correction of brain images. Neuroimage **17**(2) (2002) 825–841
7. Avants, B.B., Epstein, C.L., Grossman, M., Gee, J.C.: Symmetric diffeomorphic image registration with cross-correlation: evaluating automated labeling of elderly and neurodegenerative brain. Medical image analysis **12**(1) (2008) 26–41
8. Pierpaoli, C., Walker, L., Irfanoglu, M., Barnett, A., Basser, P., Chang, L., Koay, C., Pajevic, S., Rohde, G., Sarlls, J., et al.: Tortoise: an integrated software package for processing of diffusion MRI data. Book TORTOISE: an integrated software package for processing of diffusion MRI data (Editor eds.) **18** (2010) 1597
9. Oguz, I., Farzinfar, M., Matsui, J., Budin, F., Liu, Z., Gerig, G., Johnson, H.J., Styner, M.A.: Dtiprep: Quality control of diffusion-weighted images. Frontiers in Neuroinformatics **8** (2014) 4
10. Rohde, G.K., Barnett, A.S., Basser, P.J., Pierpaoli, C.: Estimating intensity variance due to noise in registered images: applications to diffusion tensor MRI. Neuroimage **26**(3) (2005) 673–684
11. Oishi, K., Faria, A., Jiang, H., Li, X., Akhter, K., Zhang, J., Hsu, J.T., Miller, M.I., van Zijl, P., Albert, M., et al.: Atlas-based whole brain white matter analysis using large deformation diffeomorphic metric mapping: application to normal elderly and alzheimer's disease participants. Neuroimage **46**(2) (2009) 486–499
12. Tournier, J., Yeh, C.H., Calamante, F., Cho, K.H., Connelly, A., Lin, C.P., et al.: Resolving crossing fibres using constrained spherical deconvolution: validation using diffusion-weighted imaging phantom data. Neuroimage **42**(2) (2008) 617–625
13. Garyfallidis, E., Brett, M., Amirbekian, B., Rokem, A., Van Der Walt, S., Descoteaux, M., Nimmo-Smith, I.: Dipy, a library for the analysis of diffusion MRI data. Frontiers in Neuroinformatics **8**(8) (2014)
14. Garyfallidis, E.: Towards an accurate brain tractography. PhD thesis, PhD thesis, University of Cambridge (2012)
15. Zhang, Y., Zhang, J., Oishi, K., Faria, A.V., Jiang, H., Li, X., Akhter, K., Rosa-Neto, P., Pike, G.B., Evans, A., et al.: Atlas-guided tract reconstruction for automated and comprehensive examination of the white matter anatomy. Neuroimage **52**(4) (2010) 1289–1301
16. Cohen-Adad, J., Descoteaux, M., Wald, L.L.: Quality assessment of high angular resolution diffusion imaging data using bootstrap on q-ball reconstruction. Journal of Magnetic Resonance Imaging **33**(5) (2011) 1194–1208
17. Hammond, D.K., Gur, Y., Johnson, C.R.: Graph diffusion distance: A difference measure for weighted graphs based on the graph laplacian exponential kernel. In: Global Conference on Signal and Information Processing (GlobalSIP), 2013 IEEE. (Dec 2013) 419–422
18. Landis, J.R., Koch, G.G., et al.: The measurement of observer agreement for categorical data. biometrics **33**(1) (1977) 159–174